ELSEVIER

Journal of Chromatography A, 937 (2001) 115–125

JOURNAL OF CHROMATOGRAPHY A

www.elsevier.com/locate/chroma

Flow-through sampling for electrophoresis-based microfluidic chips using hydrodynamic pumping

Yi-Hung Lin[a], Gwo-Bin Lee[b], Chun-Wei Li[c], Guan-Ruey Huang[b], Shu-Hui Chen[a,*]

[a]*Department of Chemistry, National Cheng Kung University, Tainan 701, Taiwan*

[b]*Department of Engineering Science, National Cheng Kung University, Tainan 701, Taiwan*

[c]*School of Technology for Medical Sciences, Kaohsiung Medical University, Kaohsiung 807, Taiwan*

Received 27 July 2001; received in revised form 21 September 2001; accepted 21 September 2001

Abstract

This work presents a novel electrophoretic microchip design which is capable of directly coupling with flow-through analyzers for uninterrupted sampling. In this device, a 3 mm wide sampling channel (SC) was etched on quartz substrate to create the sample inlet and outlet and the 75 μm wide electrophoretic channels were also fabricated on the same substrate. Pressure was used to drive the sample flow through the external tube into the SC and the flow was then split into outlet and electrophoretic channels. A gating voltage was applied to the electrophoretic channel to control the sample loading for subsequent separations and inhibit the sample leakage. The minimum gating voltage required to inhibit the sample leakage depended on the solution buffer and increased with the hydrodynamic flow-rate. A fluorescent dye mixture containing Rhodamine B and Cy3 was introduced into the sample stream at either a continuous or discrete mode via an on-line injection valve and then separated and detected on the microchip using laser-induced fluorescence. For both modes, the relative standard deviation of migration time and peak intensity for consecutive injections was determined to be below 0.6 and 8%, respectively. Because the SC was kept floating, the external sampling equipment requires no electric connection. Therefore, such an electrophoresis-based microchip can be directly coupled with any pressure-driven flow analyzers without hardware modifications. To our best knowledge, this is something currently impossible for reported electrophoretic microchip designs.
© 2001 Elsevier Science B.V. All rights reserved.

Keywords: Chip technology; Sample handling; Instrumentation; Rhodamine B; Sodium tetraborate; Sodium carbonate

1. Introduction

Among various microfluidic chip methods, an electrically driven chip that does not involve complicated microfabrication of pumps and valves has been found to be the most practical means to be implemented [1]. Capillary electrophoresis (CE) on microchips is an electrically-driven separation technique that is leading the next revolution in chemical analysis [1–7]. These chips allow the separation speed to reach a new milestone since the compact device configuration and, moreover, their planar structure makes it easier to achieve integrated analysis as a micro total analysis system (μTAS) or laboratory-on-a-chip.

The most common miniaturized electrophoretic chips contain two cross channels and four reservoirs for sample, sample waste, separation buffer and buffer waste. Repetitive injections can be performed

*Corresponding author. Fax: +886-6-2740-552.

E-mail address: shchen@mail.ncku.edu.tw (S.-H. Chen).

0021-9673/01/$ – see front matter © 2001 Elsevier Science B.V. All rights reserved.
PII: S0021-9673(01)01326-7

simply by voltage switching among four reservoirs [8,9]. This cross configuration allows a sample injection system to be integrated with the separation channel on a planar chip device [10]. Two major drawbacks of conventional CE are that the sample introduction method of exchanging sample and buffer reservoirs is time consuming and lacks precision. Moreover, with an electrokinetic injection scheme, ions with greater mobilities are disproportionately introduced in larger quantities. In the microfabricated device, sample loading and injection is controlled by voltage switching without physical disconnections. Furthermore, with the pinched mode loading, the volume of the sample plug can be closely controlled and is time independent, enabling the injection of a constant volume without electrophoretic mobility based bias [10]. However, the current chip design does not allow different samples to be continually introduced. A series of samples is normally introduced by mechanical pipettors [8–10], capillary forces [11], or electro-pipettors [12], and are accompanied by sequentially removing the fluid from the substrate and replacing it with another fluid. Although these procedures may be facilitated by robotic systems, the sampling rate is rather limited and cannot be linked with many flow-through analyzers [13–15]. Ramsey [16] demonstrated a new microchip functional element which is capable of electrokinetically inducing a pressure differential along the length of a channel for hydraulic pumping. This design allows both hydrodynamic and electrophoretic pressure domains on the same chip and is potentially useful for sampling. In a recent report, Attiya et al. [17] presented a chip design which allows the introduction of a continuous sample into an electrophoretic microchip without perturbing the liquids within the microfabricated device. This interface appears useful for many flow-based analyses. However, this interface requires connections for electrical grounding on the external part to create an electrical field across the external part and sampling channels on the microchip, which is infeasible for some equipments such as microdialysis. Moreover, according to our experience, such electrical connections tend to create an unstable flow in sampling channel and impair sampling, partly owing to the formation of air bubbles. On the other hand, the flow leakage problem accompanied with flow-through sampling, which may cause substantial cross contaminations, remains unsolved [17].

A novel microchip design for directly coupling electrophoretic microchips with flow-through analyzers without hardware modifications is demonstrated herein by analyzing a known compound mixture in both the continuous and discrete modes, which are conventionally used in a microdialysis probe and auto-sampling machine for high-performance liquid chromatography (HPLC), respectively. The leakage problem is reduced by applying pinching voltages in the electrophoretic manifold and is theoretically characterized.

2. Experimental

2.1. Chemicals and reagents

Sodium tetraborate decahydrate was purchased from Showa (Tokyo, Japan). Sodium carbonate and Rhodamin B were obtained from Fluka (Buchs, Switzerland), and the fluorescence dye, Cy3, was purchased from Amersham Pharmacia Biotech (Asia Pacific, Hong Kong, China). All reagents were of the highest grade available. Finally, the CE water was deionized–distilled water filtered through a Barnstead E-pure system, and had a resistance of over 18.0 MΩ/cm.

2.2. Microchip and instrumentation

The device configuration is depicted in Fig. 1. The 3 mm wide channel (between A and B) was the sampling channel (SC), while the remaining channels have a width of 80 μm, and where all channels have a depth of 40 μm. The microchip was fabricated on a quartz substrate using standard photolithography techniques in a microsystem laboratory at National Cheng Kung University. Before bonding, six through holes (A–F) with a diameter of 1.5 mm were mechanically drilled on the cover plate. Holes C–F were used as reservoirs while holes A and B were used as sample inlets and outlets. The schematic diagram of the instrumental set-up is displayed in Fig. 2. For the continuous mode, holes A and B were glued to a PTFE tubing (250 μm I.D.×1/16 in. O.D.; 1 in.=2.54 cm) and a syringe

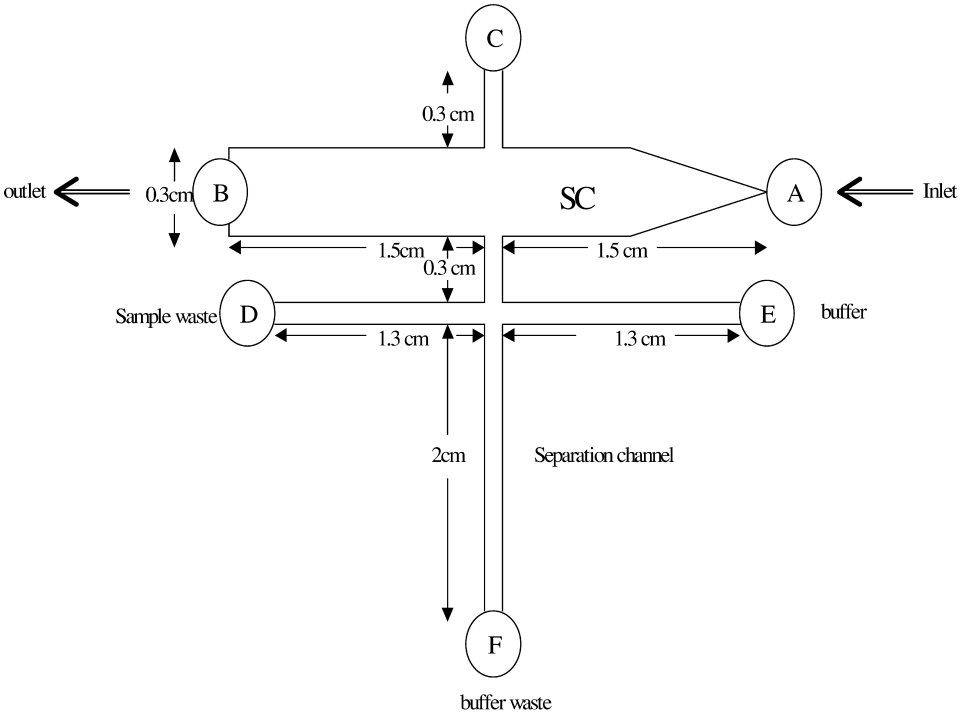

Fig. 1. Channel configuration of the microchip. Holes A–F were drilled on the cover plate, A and B were glued to a PTFE tubing for transporting hydrodynamic flow, and holes C–F were used as buffer reservoirs. See text descriptions.

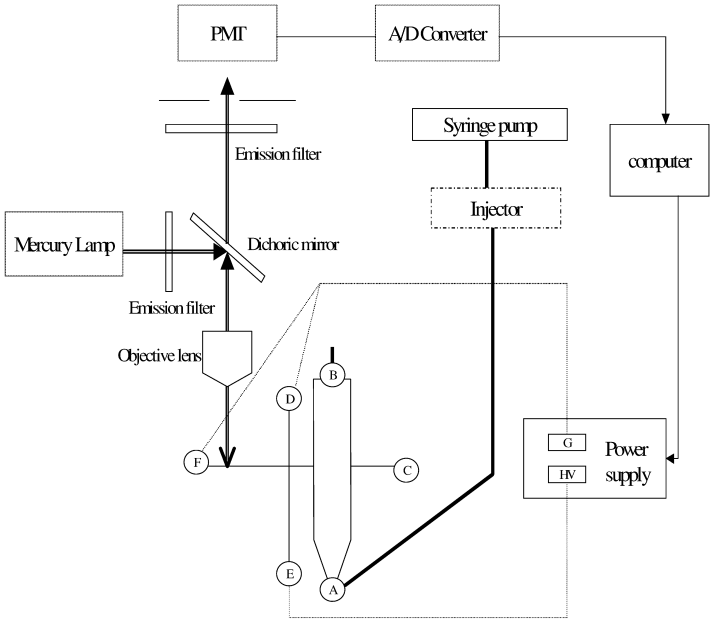

Fig. 2. Schematic diagram of the microchip's detection and power supply systems. Dashed lines denotes the light path, the bold line represents PTFE tubing, and the normal line indicates electrical connections.

pump (Series 74900, Cole Parmer, Vernon Hills, IL, USA) was used to drive the flow through the tubing into A and then from the outlet B to a waste vial. Although some dead volume could exist in the PTFE fitting on the chip, this will not influence the separation efficiency since the dead volume exists before the sample injection. For the discrete mode, a 60-nl injection valve (Valco Instruments, Houston, TX, USA) was placed in series between the microchip and the syringe pump (Fig. 2) and a PTFE tubing (125 μm I.D.×1/16 in. O.D.) smaller than that used in the continuous mode was utilized for hydrodynamic flow transport to minimize the dilution effect. Three platinum electrodes were inserted into reservoirs D, E, and F (Fig. 2), respectively. A high-voltage power supply (Series 230, Bertan High Voltage, Hicksville, NY, USA) was employed to furnish the loading and separation voltages and the power switching was controlled by a program written with LabVIEW (National Instruments, Austin, TX, USA) running on a Pentium 75 MHz computer. Signals were detected on-microchip via fluorescence detection, with the detection system being constructed by modifying a commercial reflection microscope (Model BX40, Olympus, Tokyo, Japan) [8]. Briefly, a mercury lamp was focused on the microchannel at specified positions using a 50× (NA= 0.5) long working distance objective. Fluorescence was collected by the same objective lens and passed through a dichroic cube with a band-pass filter, followed by spatial filtering and finally detected by a photomultiplier tube (PMT) operated at −650 V (R928, Hamamatsu, Tokyo, Japan) or a charged-coupled device (CCD) camera depending on the experimental need. Amplified photoelectron signals were converted to the digital signal and processed by a computer using a commercial interface (Model 9524, SISC, Taipei, Taiwan) running on the same computer as for voltage switching.

2.3. Voltage switching scheme

Fig. 3 illustrates the voltage switching scheme for the sample introduction. First, a high positive voltage which was regarded as the gating voltage was applied to reservoir E, while reservoirs D and F were grounded (Fig. 3A and B). Under this voltage scheme, the inlet flow was split in the first manifold and then pinched to reservoir D through the second manifold. For sample loading (Fig. 3C), reservoirs D, E, and F were set to float for a specified period which determined the quantity of the sample to be analyzed in the separation channel. For sample separation (Fig. 3D), reservoirs D and F were immediately grounded and the positive high voltage which was regarded as the separation voltage was applied to reservoir E to initiate sample separation. According to this voltage-gating scheme, reservoir C seems unnecessary since no electrode or voltage is applied to it. However, the presence of reservoir C is helpful for vacuum cleaning and for normal separation when only the simple cross portion of the chip is used.

3. Results and discussion

The proposed sample flow during voltage-gated loading and separation can be experimentally verified from the CCD images taken near the cross region during sampling (Fig. 4). As a pinching voltage was applied to reservoir E (Fig. 3B), the sample flow was directed to reservoir D (Fig. 4A). In the next moment, when all electrodes were set to float for a specified period of loading time (Fig. 3C), a certain quantity of sample flowed into the channels (Fig. 4B). Subsequently, as the separation voltage was applied to reservoir E and reservoirs D and F were grounded (Fig. 3D), a sample plug was loaded (Fig. 4C) and migrated (Fig. 4D) along the separation channel. This loading method also compensated for electrophoretic bias since the electrophoresing materials entered the separation channel by pressure-driven flow rather than electrophoretic forces. Under this voltage scheme, the SC was kept floating throughout the whole process during which the gating or separation voltage was applied to other channels. For unknown reasons, this voltage scheme was found to provide a stable flow in the SC for a longer period of time compared to other schemes in which a high voltage was applied to reservoirs A or C. When a gating voltage was applied between A and D or C and D, the electrical current is unstable and air bubbles were frequently formed in SC channel. These have made the sampling become impossible, possibly due to unequal channel diameters between

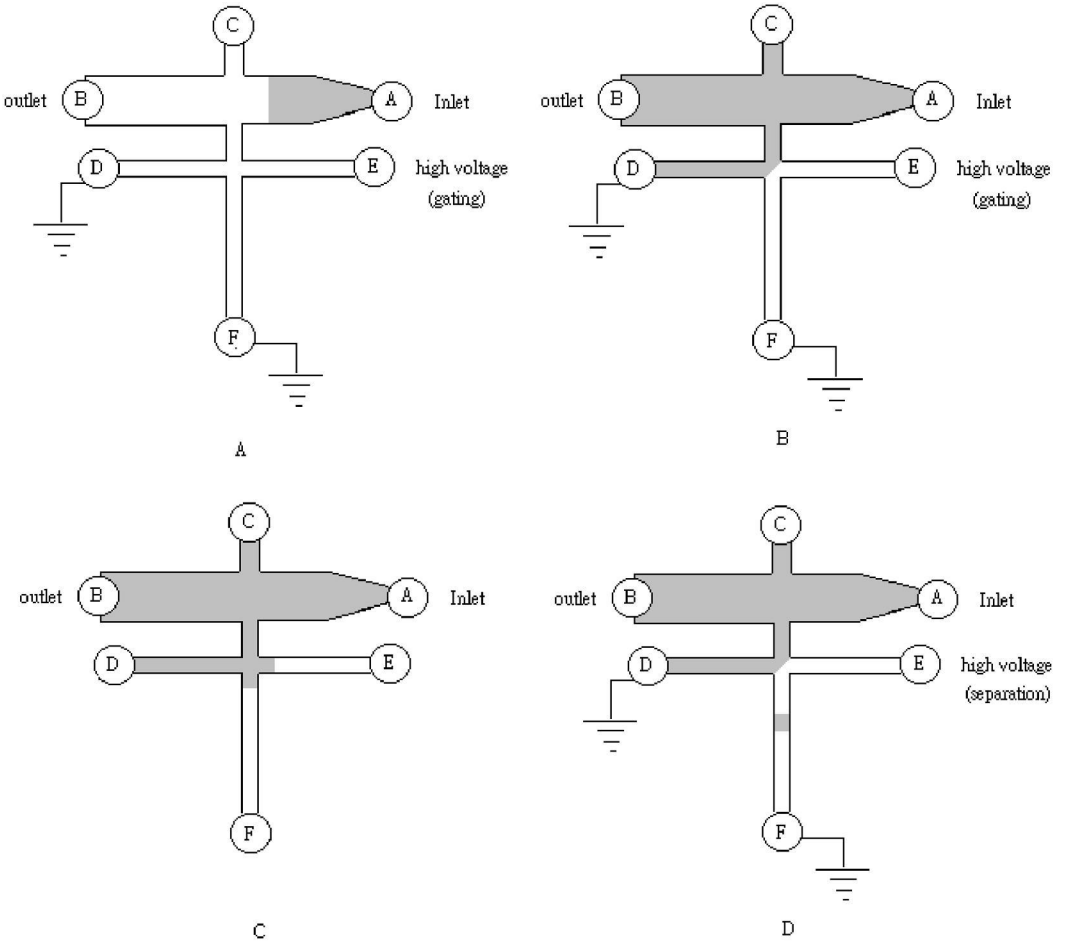

Fig. 3. Voltage switching scheme for sample introduction. See text descriptions. The high voltage values and the running buffers are indicated with each electropherogram.

SC and the electrophoretic channel and thus different flow resistance. This scheme allowed reproducible samplings for over 20 min. If the increased liquids in reservoirs D and F can be removed and reservoir E can be refilled, the sampling time will increase. Moreover, the flow bias caused by capillary forces due to unbalanced liquid levels in reservoirs can also be minimized [18].

3.1. Critical gating voltage

As mentioned earlier, the sampling microdevice is based on hydrodynamic sample splitting followed by voltage-gated injection. The SC not only forms an open loop for flow-through analysis, but also provides the device with two functions. First, the sample stream was split in the microchip such that the injection volume can be reduced to the nl range, thus achieving an efficient separation through capillary electrophoresis, of course, the quantity of the waste increases with the split ratio. Second, the hydrodynamic volume flow-rate in the split channel can be largely reduced, thus allowing the required gating voltage to be lowered. During voltage-gated injection, the applied pinching voltage must be sufficient to inhibit flow from moving to the separation channel. Otherwise, the leakage of analytes into the separation channel will increase the background

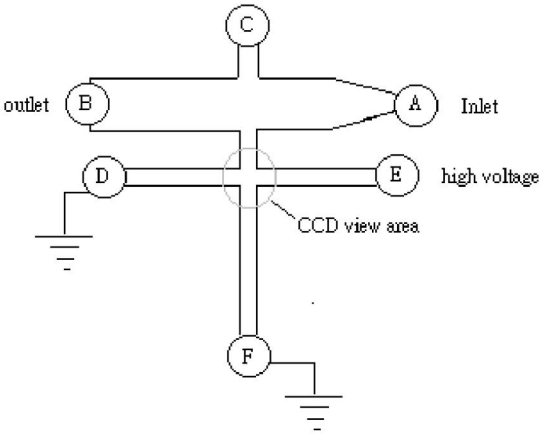

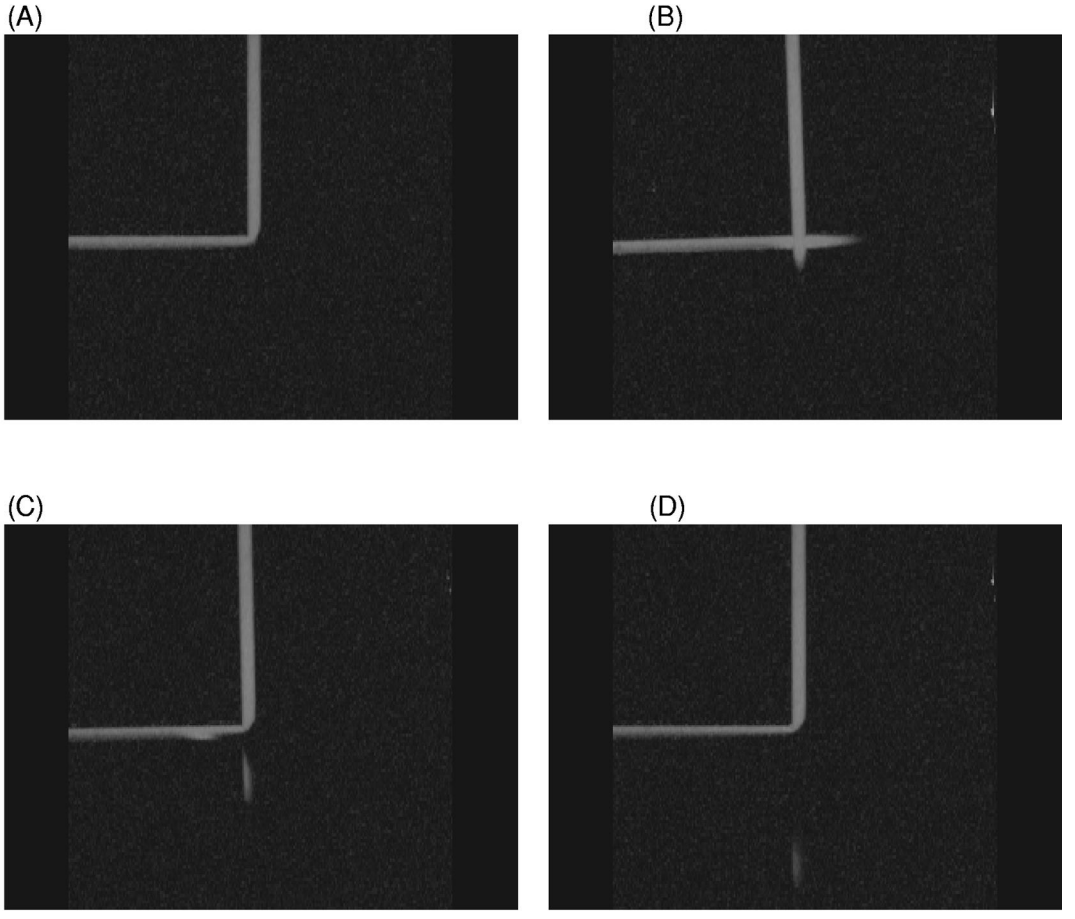

Fig. 4. The CCD images of the sample flow containing Rhodamine B ($4 \cdot 10^{-5}$ *M* in 20 m*M* sodium tetraborate, pH 9.2) at a hydrodynamic flow-rate of 5 μl/min. The A, B, C images, respectively, corresponded to B, C, D of Fig. 3. The applied pinching voltage (A) and separation voltage (C and D) were both 1.5 kV, and the loading time with electrodes D, E, and F floating (B) was 1.5 s.

signal. On the other hand, using a higher gating voltage could also minimize the backflow owing to the capillary force which arises when liquid levels on reservoirs differ significantly [18].

To determine the required gating voltage at which the hydrodynamic and electroosmotic forces were balanced, both the applied gating voltage and hydrodynamic flow-rate were systematically varied. For this investigation, the gating voltage was applied to reservoir E after the loading; in other word, the sequence step B illustrated in Fig. 3 was deleted and the separation voltage indicated in Fig. 3D was regarded as the gating voltage. Under this operation, the signal first increased as the flow reached the detection point and then decreased instantly as a pinching was applied to reservoir E. However, a leakage background will be detected if the gating voltage was not sufficient to inhibit the flow. As shown in Fig. 5, at a hydrodynamic flow-rate of 2 μl/min, a tailing background developed as the gating voltage was lowered to 0.7 kV. The CCD image taken at a gating voltage of 0.5 kV clearly indicates that a certain quantity of sample leaked into the separation channel (Fig. 5). If the electroosmotic flow-rate is equal to or exceeds the hydrodynamic flow-rate, the signal will be suppressed to the background level. The critical gating voltage was thus defined as the lowest voltage at which the leakage signal was less than three times of the noise signal. The plots of the critical gating voltage versus

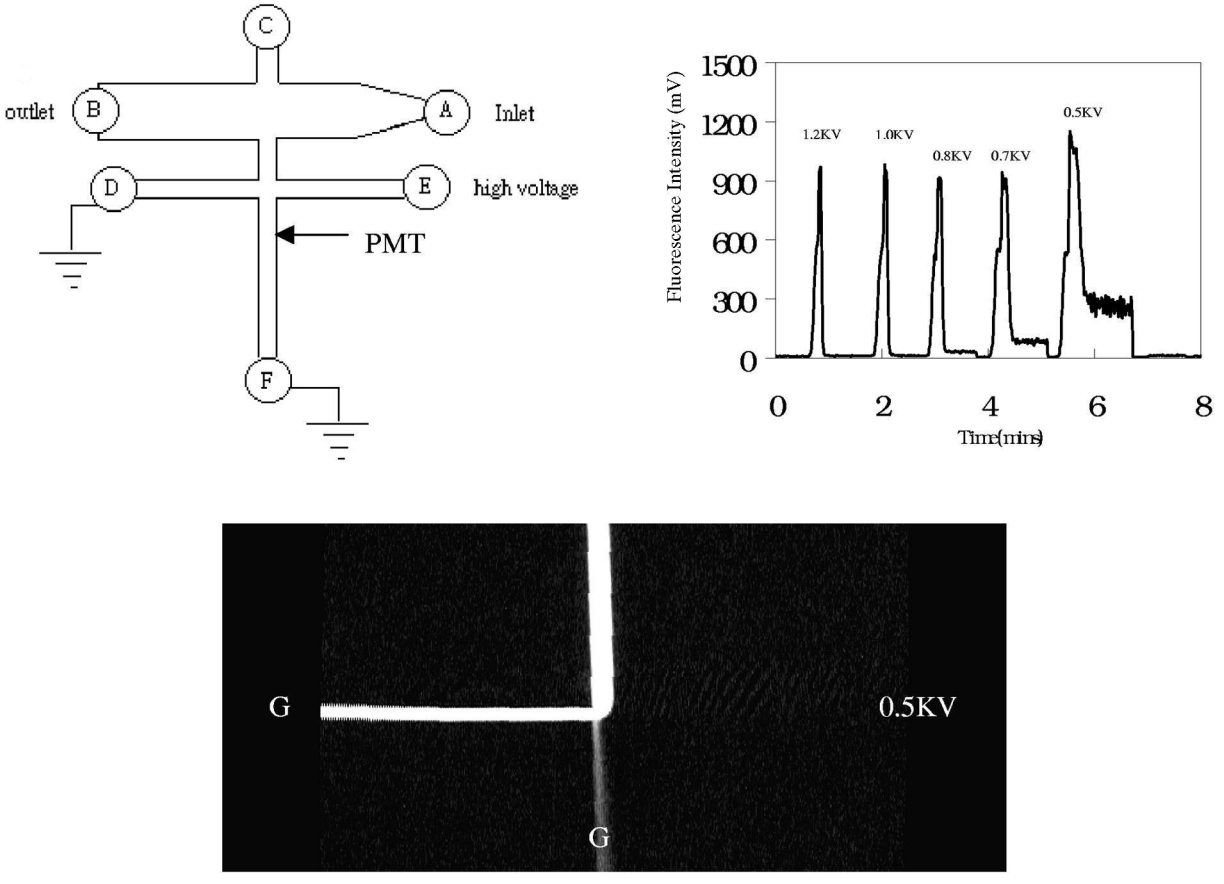

Fig. 5. The effect of gating voltage. In the top figure, pinching voltages of 1.2, 1.0, 0.8, 0.7, and 0.5 kV were applied to reservoir E and the PMT was placed along the separation channel, 1.6 cm from the second cross. See Results and discussion section for detailed operation descriptions. The bottom CCD image around the second cross (same position as in Fig. 4) was taken at a gating voltage of 0.5 kV and the sample leakage was clearly indicated.

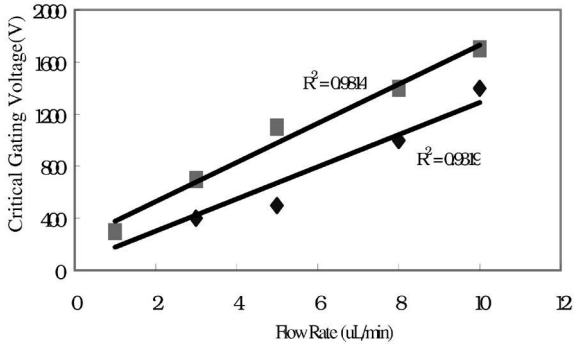

Fig. 6. The effect of hydrodynamic flow-rate on the critical gating voltage. The data were acquired with two separation buffers: sodium tetraborate, pH 9.2 (■) and sodium carbonate, pH 11.5 (♦).

the hydrodynamic flow-rate under two buffer systems were shown in Fig. 6 and their linear regression lines were also indicated. Although the R^2 values were below 0.99, the slope of the linear plots appears to vary with the buffer. The parameters which effect the critical gating voltage under a constant hydrodynamic flow-rate may be theoretically deduced. The volumetric flow-rate owing to electroosmosis, v_{os}, is related to electroosmotic mobility, μ_{os} and the electric field, E, as indicated in Eq. (1) [19]:

$$v_{os} = \mu_{os} ES \tag{1}$$

in which S denotes the cross-sectional area of the channel and E can be expressed as the quotient of the applied voltage, V, divided by the length of the channel, L:

$$v_{os} = \mu_{os}(V/L)S = KV \tag{2}$$

In Eq. (2), K is equal to $\mu_{os}S/L$. At a critical gating voltage, the volumetric flow-rate due to electroosmosis, v_{os}, and the volumetric flow-rate due to hydrodynamic force (pressure gradient), F, should be balanced:

$$F = v_{os} = KV \tag{3}$$

$$V = F/K \tag{4}$$

Eq. (4) displays that F is linearly related to V as long as the slope, $1/K$, is a constant. The value, K, is dependent on the channel geometry (LS) and μ_{os}. Meanwhile, electroosmotic mobility, μ_{os}, is proportional to the surface charge density (σ^*), the double layer thickness, κ^{-1}, and inversely proportional to the viscosity of the solution (η) [19]:

$$\mu_{os} = \sigma^* \kappa^{-1}(\epsilon, C_i)/\eta \tag{5}$$

The double layer thickness, κ^{-1}, is a function of the electrical permittivity of the solvent, ϵ, and the ionic concentration of the buffer, C_i. Apparently, some parameters such as σ^* and κ^{-1} could have been changed after several runs, leading to the deviation of the linearity shown in the bottom plot of Fig. 6. We have also investigated the gating phenomena (Fig. 5) many times and found to be consistent except that the absolute value of critical gating voltage for a specific flow-rate appeared to increase gradually with the time, which could be due to the modification of the channel wall after use as well. Clearly, an efficient washing step before run needs to be included in the operation sequence. Nevertheless, the plots in Fig. 6 reveal that the slope for sodium tetraborate buffer (pH 9.2) is slightly greater than that for sodium carbonate buffer (pH 11.5). Since the ionic concentration of two buffer systems was equal, this difference could be due to the smaller pH value of sodium tetraborate butter, causing a smaller surface charge density, σ^*, a smaller μ_{os}, a greater $1/K$ and a steeper plot slope. The calculation of the theoretical gating voltage requires accurate measurements of μ_{os}, which is currently ongoing.

The capability of the microchip for continuous sampling was demonstrated through analyzing a known compound and a compound mixture in both the continuous and discrete modes.

3.2. Continuous mode of sample introduction

In the continuous mode, the compound was continuously delivered to SC on the chip using a syringe pump under an isocratic or gradient condition. This mode resembles the sampling method used for a microdialysis probe. As shown in Fig. 7A, under an isocratic condition, consistent signals were detected for consecutive injections at a sampling rate of 12 s per injection. Meanwhile, under a step gradient condition (Fig. 7B), the signal intensity was increased with the concentration of Rhodamin B in the hydrodynamic flow stream. In addition to sample

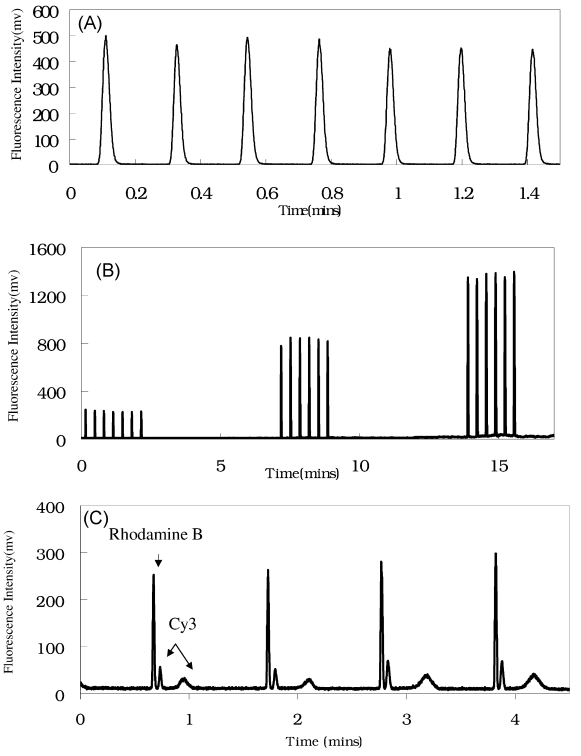

Fig. 7. Consecutive injections of the continuous mode. (A) The sample flow contained Rhodamine B ($4 \cdot 10^{-5}$ *M* in 20 m*M* sodium tetraborate, pH 9.2) at a hydrodynamic flow-rate of 2 μl/min. The applied gating and separation voltages were both 0.8 kV and the loading time was 1.5 s. (B) The concentration of Rhodamine B in the sample flow was varied by mixing two syringe pumps containing 10^{-5} and 10^{-6} *M* of Rhodamine B, respectively. The final concentrations in the sample flow were 10^{-6}, $5 \cdot 10^{-5}$ and 10^{-5} *M* for the first, second, and third series of consecutive injections, respectively, at a hydrodynamic flow-rate of 5 μl/min. The applied gating and separation voltages were both 1.4 kV and the loading time was 2.0 s. (C) The sample flow contained Rhodamine B (10^{-5} *M*) and Cy3 ($6.5 \cdot 10^{-5}$ *M*) in 20 m*M* sodium carbonate buffer (pH 11.5) at a hydrodynamic flow-rate of 7 μl/min. The applied gating and separation voltages were both 1.3 kV and the loading time was 1.0 s.

injection, the integration of sample introduction and separation was further demonstrated by introducing a mixture of Rhodamin B and Cy3 fluorescence dyes. As displayed in Fig. 7C, Rhodamine B was first eluted and Cy3 was eluted as a sharp peak and a broad band, which could be due to the hydrolyzed species since Cy3 was unstable in an aqueous solution. Consecutive sample introduction and separation was achieved in under 1 min, with relative standard deviations of peak intensity and average migration time less than 7.6 and 0.64%, respectively (Fig. 7C). It was found that the reproducibility was degraded with time as discussed previously and is expected to be resumed as the liquid in reservoir D is removed and the channel walls are cleaned. Moreover, the effect of the pressure-driven flow on the band broadening of the separated peaks is expected to be minimum since the pressure is estimated to be small (tens of p.s.i.; 1 p.s.i. = 6894.76 Pa) and the hydrodynamic flow in the separation channel is inhibited by the gating voltage.

3.3. Discrete mode of sample introduction

The capability of the device for sample introduction was further investigated under a discrete mode normally used for chromatographic analysis. In this mode, discrete samples were introduced into the flow stream via an injection valve connected on-line to the flow stream. Sampling was achieved through time coordination between the injection valve and voltage switching system. This process can be easily automated through proper software control, although the system is currently lack of this capability and all injections were manually controlled. Although the Valco injection valve introduced a sample plug of 60 nl, it is estimated that only one tenth of the introduced sample was injected into the electrophoretic channel based on the the relative channel diameter. In Fig. 8A, semi-quantitative results were revealed as samples with different concentrations were injected. The integration of sample introduction and separation was further demonstrated in Fig. 8B as a mixture of Rhodamin B and Cy3 fluorescence dyes was introduced into the separation channel. Reproducible signals with a relative standard deviation of peak intensity below 6% for each concentration were obtained when electro-gating was applied for the sampling. The sampling rate for the discrete mode can be further increased as the system is automated in the future.

4. Conclusions

A microfabricated device is demonstrated herein to be capable of non-interrupted and reproducible

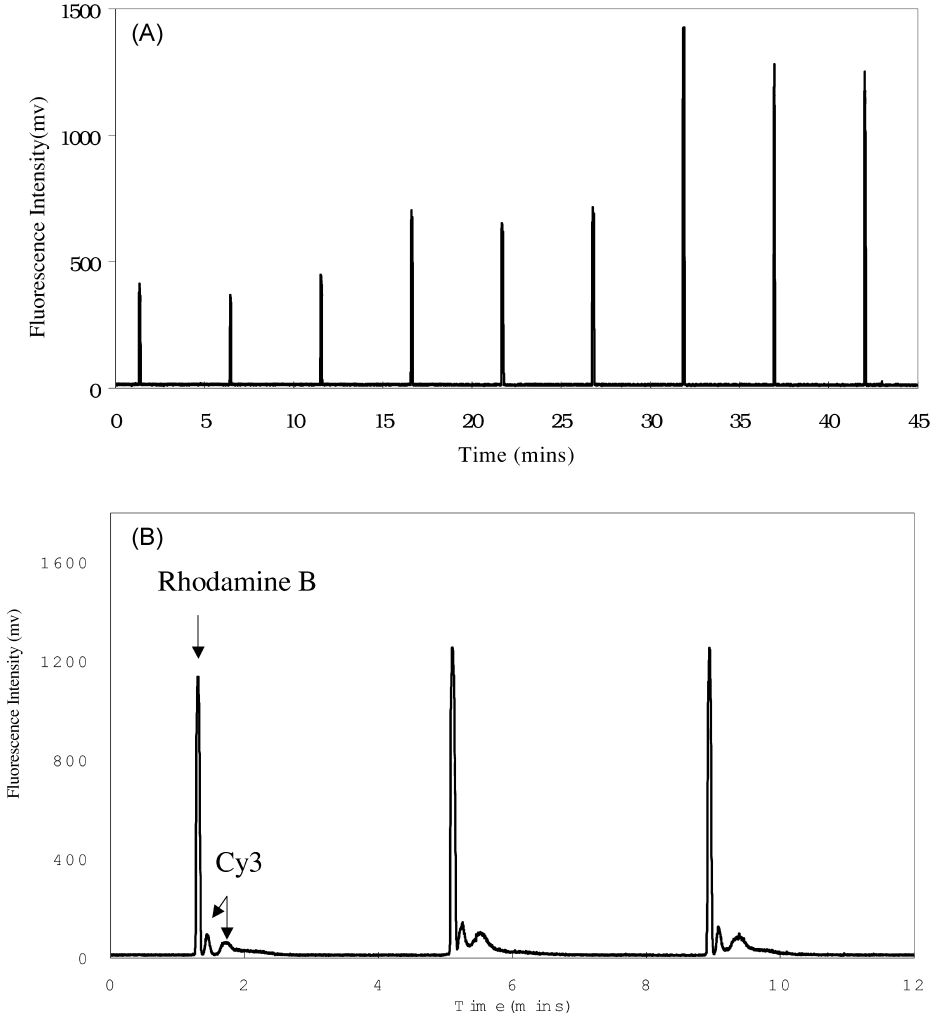

Fig. 8. Consecutive injections of the discrete mode. (A) The concentrations of the injected Rhodamine B (via a 60-nl injection valve) in 20 m*M* sodium tetraborate, pH 9.2 were $2.5 \cdot 10^{-5}$, $5 \cdot 10^{-5}$, and 10^{-4} *M* for the first, second, and the third consecutive injections, respectively. Meanwhile, the hydrodynamic flow-rate was 5 μl/min, the applied gating and separation voltages were both 1.3 kV and the loading time was 12 s. (B) The injected sample contained Rhodamine B ($3 \cdot 10^{-5}$ *M*) and Cy3 ($6.5 \cdot 10^{-4}$ *M*) in 20 m*M* sodium carbonate buffer (pH 11.5) at a hydrodynamic flow-rate of 5 μl/min. The applied gating and separation voltages were both 1.3 kV and the loading time was 3.0 s.

sample introduction, separation, and detection from either a continuous flow or discrete sample zones in a continuous flow stream. These capabilities would allow direct coupling between the electrophoresis-based microchip and many flow-through analyzers, such as a microdialysis probe and the auto-sampling machine for liquid chromatography. System automation is now being sought to achieve a rapid and high throughput flow analysis system.

Acknowledgements

Financial support from National Science Council

of Taiwan (NSC 89-2323-B-006-008) and the microsystem laboratory of National Cheng Kung University are greatly acknowledged.

References

[1] D.J. Harrison, K. Fluri, K. Seiler, Z. Fan, C.S. Effenhauser, A. Manz, Science 261 (1993) 895.
[2] A. Manz, D.J. Harrison, E.M.J. Verpoorte, J.C. Fettinger, A. Paulus, H. Ludi, H.M. Widmer, J. Chromatogr. 593 (1992) 253.
[3] D.E. Raymond, A. Manz, H.M. Widmer, Anal. Chem. 66 (1994) 2858.
[4] F.E. Regnier, B. He, S. Lin, J. Busse, Trends Biotechnol. 17 (1999) 101.
[5] C.S. Effenhauser, A. Paulus, A. Manz, H.M. Widmer, Anal. Chem. 66 (1994) 2949.
[6] S.H. Chen, LC–GC Mag. (Europe) 13 (2000) 766.
[7] Y.H. Chen, W.C. Wang, K.C. Young, T.T. Chang, S.H. Chen, Clin. Chem. 45 (1999) 1938.
[8] Y.H. Chen, S.H. Chen, Electrophoresis 21 (2000) 165.
[9] C.S. Effenhauser, A. Manz, H.M. Widmer, Anal. Chem. 65 (1993) 2637.
[10] S.C. Jacobson, R. Hergenroder, L.B. Koutny, R.J. Warmack, J.M. Ramsey, Anal. Chem. 66 (1994) 1107.
[11] S.A. Sundberg, J.W. Parce, C.Y.H. Chow, US Pat. 6 090 251 (2000).
[12] J.W. Parce, M.R. Knapp, US Pat. 6 042 709 (2000).
[13] B.L. Hogan, S.M. Lunte, J.F. Stobaugh, C.E. Lunte, Anal. Chem. 66 (1994) 596.
[14] M.W. Lada, R.T. Kennedy, Anal. Chem. 68 (1996) 2790.
[15] M.W. Lada, T.W. Vickroy, R.T. Kennedy, Anal. Chem. 69 (1997) 4560.
[16] J.M. Ramsey, Anal. Chem. 72 (2000) 2285.
[17] S. Attiya, A.B. Jemere, T. Tang, G. Fitzpatrick, K. Seiler, N. Chiem, D.J. Harrison, Electrophoresis 22 (2001) 318.
[18] H.J. Crabtree, D.A. Tilroe, E.C.S. Cheong, C.J. Backhouse, presented at the 14th International Symposium on Microscale Separations and Analysis, Boston, MA, 13–18 January 2001, poster 90309 M.
[19] P.D. Grossman, in: P.D. Grossman, J.C. Colburn (Eds.), Capillary Electrophoresis, Academic Press, San Diego, CA, 1992, p. 3.